

TIME-DEPENDENT PHOTON CORRELATIONS FOR INCOHERENTLY PUMPED QUANTUM DOT STRONGLY COUPLED TO THE CAVITY MODE

*A. V. Poshakinskiy**, *A. N. Poddubny*

*Ioffe Physical-Technical Institute, Russian Academy of Sciences
194021, St. Petersburg, Russia*

Received September 25, 2013

The time dependence of correlations between the photons emitted from a microcavity with an embedded quantum dot under incoherent pumping is studied theoretically. Analytic expressions for the second-order correlation function $g^{(2)}(t)$ are presented in strong and weak coupling regimes. The qualitative difference between the incoherent and coherent pumping schemes in the strong coupling case is revealed: under incoherent pumping, the correlation function demonstrates pronounced Rabi oscillations, but in the resonant pumping case, these oscillations are suppressed. At high incoherent pumping, the correlations decay monoexponentially. The decay time nonmonotonically depends on the pumping value and has a maximum corresponding to the self-quenching transition.

DOI: 10.7868/S0044451014020059

1. INTRODUCTION

Semiconductor quantum dots form a promising platform for quantum optics devices, including single-photon emitters and emitters of entangled photon pairs [1–4]. The quantum dot-based light sources can be characterized by means of photon–photon correlation spectroscopy, i. e., by measuring the second-order correlation function $g^{(2)}(t)$ between two photons with a delay t [5, 6]. Multiple experimental observations of the antibunching [$g^{(2)}(0) < 1$] of the photons emitted from quantum dots are already available [7–11]. One of the possible routes to further enhancing the performance of these light sources is to resonantly couple the quantum dot exciton to the photon mode confined inside the microcavity in all three spatial directions [3]. The physics of such quantum microcavities becomes especially rich in the strong-coupling regime, where the new quasiparticles, exciton polaritons, are formed due to the interaction between excitons and cavity photons [1, 3, 12–15].

Here, we study the time dependence of the second-order correlations between the photons emitted from a quantum dot microcavity under stationary incoherent pumping. Experimentally, this regime can be re-

alized in quantum dot microcavities driven by electrical pumping [16] or continuous optical pumping [14]. The coexistence of (i) the strong-coupling regime and (ii) the stationary incoherent pumping regime makes the time dynamics of the correlations very specific.

The strong-coupling regime [17–19] qualitatively distinguishes the system from the conventional laser, described by the Scully–Lamb theory [20]. Moreover, the incoherent pumping makes it different from the single-atom laser in the strong-coupling regime, which has been demonstrated experimentally and analyzed theoretically [21, 22]. Such systems are typically coherently pumped by resonant light [4, 23–26]. As we show in Sec. 3, the photon–photon correlations for a resonantly pumped atom and for an incoherently pumped quantum dot are very different. While both systems show antibunching, the time-dependent correlator $g^{(2)}(t)$ demonstrates oscillations at the vacuum Rabi splitting frequency in the incoherent pumping case, but not in the case of a resonantly pumped atom [21]. Recent experiments for incoherently pumped laser with a single quantum dot in the strong-coupling regime [14], as well as the comprehensive theoretical analysis in [27–29], were focused on the stationary correlator $g^{(2)}(0)$ at zero time delay. Detailed analysis of time-dependent correlations was limited to the regime with a large exciton–photon detun-

*E-mail: poshakinskiy@mail.ioffe.ru

ing [30, 31] or weak coupling [10], where the polaritons are not formed.

Hence, there is still a need to develop a detailed theory accounting for the specifics of the fast-increasing field of quantum-dot-based cavity quantum electrodynamics. Here, we focus on the temporal dynamics of correlations in the strong-coupling regime and show that it provides additional information on the lifetime of polariton eigenstates and the energy splitting between them. Our main goal is to derive transparent analytic answers for the time-resolved correlator $g^{(2)}(t)$ as a function of the incoherent pumping intensity in both strong and weak coupling regimes.

The rest of the paper is organized as follows. In Sec. 2, the model and the calculation approach are described. Section 3 is devoted to the role of the pumping mechanism and demonstrates the difference between incoherent and resonant pumping schemes. Sections 4 and 5 respectively present the theory developed in the strong and weak coupling regime. The results are summarized in Sec. 6. Auxiliary derivations are given in Appendices A and B.

2. MODEL

We consider a zero-dimensional microcavity where a single photon mode is coupled to a single exciton state of the quantum dot. Polarization degrees of freedom of both photons and excitons are disregarded for simplicity. Under these assumptions, the Hamiltonian of the system has the standard form [1]

$$H = \hbar\omega_0 c^\dagger c + \hbar\omega_0 b^\dagger b + \hbar g(c^\dagger b + cb^\dagger), \quad (1)$$

where ω_0 is the resonance frequency of the cavity, tuned to the exciton resonance, c and c^\dagger are the boson annihilation and creation operators for the cavity mode ($[c, c^\dagger] = 1$), $b = |G\rangle\langle X|$ and $b^\dagger = |X\rangle\langle G|$ are the corresponding operators for the single-exciton mode, $|X\rangle$ and $|G\rangle$ are respective states with one exciton and no excitons, and g is the light–exciton coupling constant. Equation (1) corresponds to a quantum dot smaller than the exciton Bohr radius. To consider the case of a large quantum dot, one should generalize the model following Refs. [32, 33].

To determine the intensity of emission from the cavity, we should also introduce the processes of particles generation and decay. We consider incoherent continuous pumping of excitons into the quantum dot with the rate W (see Fig. 1a). The “microscopic” discussion of the pumping mechanism can be found in Ref. [32], while the distinction between incoherent and coherent

pumping schemes is discussed in Sec. 3. The exciton mode is characterized by the nonradiative damping Γ_X . Photons can escape the cavity through the mirrors with the rate Γ_C . Hence, the full system state is described by a density matrix ρ and its evolution is determined by the equation $d\rho/dt = \mathcal{L}[\rho]$ with the Liouvillian [1]

$$\mathcal{L}[\rho] = -\frac{i}{\hbar}[H, \rho] + \Gamma_C L_c[\rho] + \Gamma_X L_b[\rho] + W L_{b^\dagger}[\rho], \quad (2)$$

where $L_a[\rho] = (2a\rho a^\dagger - a^\dagger a\rho - \rho a^\dagger a)/2$ are the Lindblad terms, accounting for damping and pumping. The stationary density matrix ρ_0 satisfies the equation $\mathcal{L}[\rho_0] = 0$. We can calculate the number of photons in the cavity $N_C = \langle c^\dagger c \rangle$ and the exciton occupation number $N_X = \langle b^\dagger b \rangle$ as

$$N_C = \text{Tr}(c^\dagger c \rho_0), \quad N_X = \text{Tr}(b^\dagger b \rho_0), \quad (3)$$

where Tr stands for the operator trace and angular brackets denote the quantum mechanical expectation value. The luminescence spectrum of the system is given by [5]

$$I(\omega) \propto \text{Re} \int_0^\infty dt e^{i\omega t} \langle c^\dagger(0)c(t) \rangle. \quad (4)$$

A detailed study of the dependence of these first-order correlators on the pumping and on other parameters can be found in Refs. [28, 34]. The goal of this paper is to analyze the time dependence of the second-order correlator that characterizes fluctuations of the emission intensity from the cavity. They are described by the correlator $g^{(2)}(t)$ determining the probability to register two photons with the time delay t [5]:

$$g^{(2)}(t) = \frac{1}{N_C^2} \langle c^\dagger(0)c^\dagger(t)c(t)c(0) \rangle. \quad (5)$$

Equation (5) presents the simplest definition of the correlation function, suitable for the analytic treatment in what follows. A more general expression, taking the finite response rate and spectral window of the photon detector for two- and multiple-photon correlations into account is given in Ref. [6]. The calculation of $g^{(2)}(t)$ is based on the quantum regression theorem [5]

$$g^{(2)}(t) = \frac{1}{N_C^2} \text{Tr}[c^\dagger c \chi(t)], \quad (6)$$

where the evolution of the operator $\chi(t) \equiv e^{\mathcal{L}t}[c\rho_0 c^\dagger]$ is governed by the dynamic equation

$$\frac{d\chi}{dt} = \mathcal{L}[\chi], \quad \chi(0) = c\rho_0 c^\dagger. \quad (7)$$

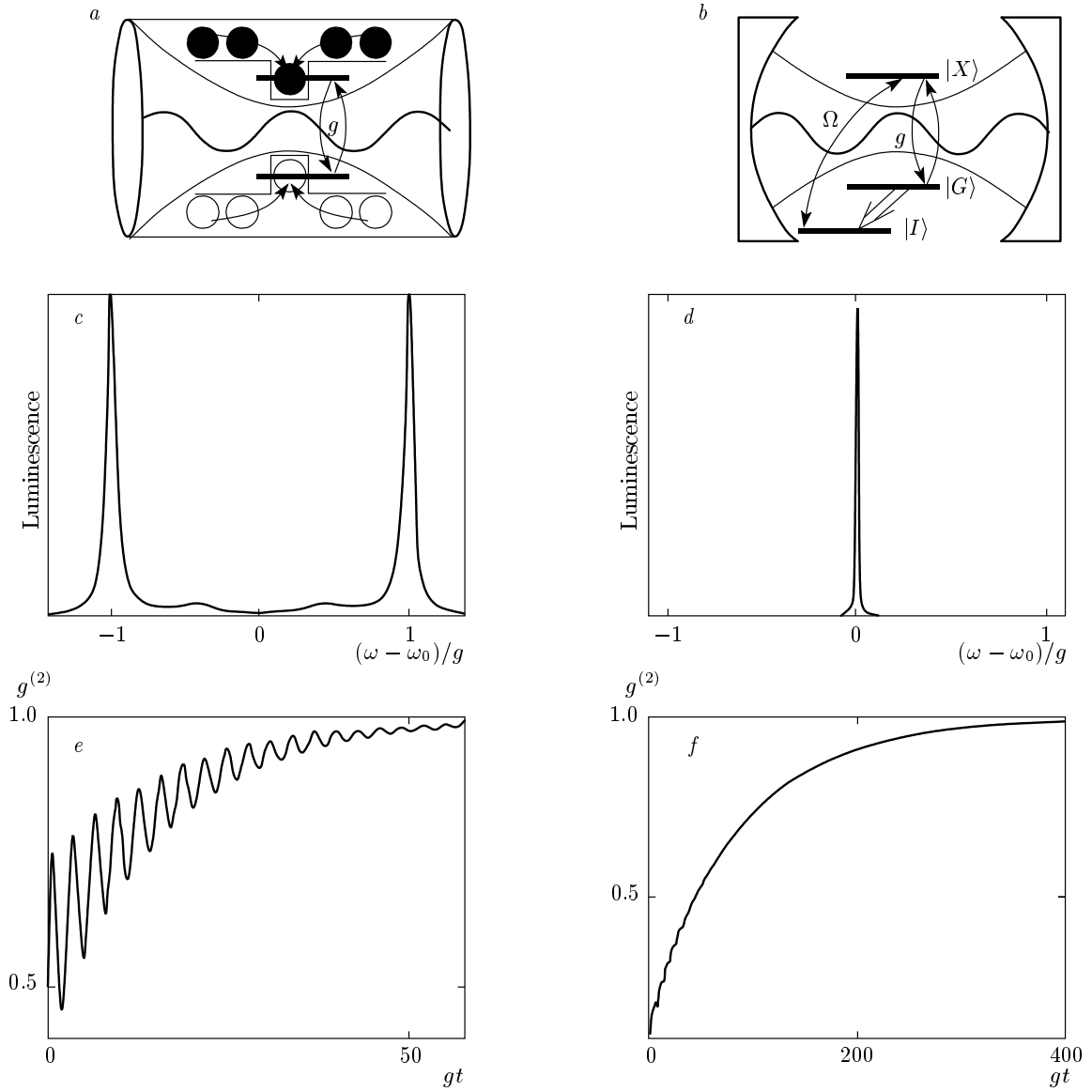


Fig. 1. The sketch of (a) an incoherently pumped quantum dot in a microcavity system and (b) a resonantly pumped 3-level atomic cavity system. Panels c and d show the comparison of the luminescence spectra for these systems, while panels e and f present the $g^{(2)}(t)$ dependence. The parameters chosen are $g/\Gamma_C = 10$, $\Gamma_X = 0.1\Gamma_C$, and $W/\Gamma_C = 0.1$ for the quantum dot in the microcavity system (panels c,e) and $g/\Gamma_C = 10$, $\Gamma_X = \Gamma_{IX} = \Gamma_{IG} = 0.1\Gamma_C$ and $\Omega/2g = 0.01$ for the atomic cavity system (panels d,f)

For zero time delay, Eq. (6) assumes the form

$$g^{(2)}(0) = \frac{1}{N_C^2} \text{Tr}(c^\dagger c^\dagger c c \rho_0). \quad (8)$$

For large time delays, the correlator tends to unity, $g^{(2)}(t \rightarrow \infty) = 1$, because the probabilities of detection of two photons become independent.

3. COMPARISON OF INCOHERENT AND COHERENT PUMPING

In this section, we compare the characteristics of emitted photons in the cases of coherent and incoherent pumping. We focus on the strong-coupling regime, when the light–exciton coupling g is stronger than the decay rates of the exciton and photon. We demonstrate below that these two pumping schemes are qual-

itatively different even at a small pumping rate. The incoherent pumping scheme is used for the quantum dot in a microcavity as sketched in Fig. 1*a* and was described in Sec. 2. The density matrix equations can be conveniently analyzed using the basis of eigenstates of Hamiltonian (1), which are well defined in the strong-coupling regime ($g \gg \Gamma_C, \Gamma_X$). The eigenstates are given by [35]

$$|0\rangle = |0, G\rangle, \quad |m, \pm\rangle = \frac{|m, G\rangle \pm |m-1, X\rangle}{\sqrt{2}}, \quad (9)$$

$$m \geq 1,$$

where $|m, G\rangle$ and $|m, X\rangle$ are the respective states with m photons and no excitons or one exciton. The energy spectrum forms the Jaynes–Cummings ladder

$$E_0 = 0, \quad E_{m,\pm} = m\hbar\omega_0 \pm \sqrt{m}\hbar g. \quad (10)$$

Each rung of the ladder contains two states split by the Rabi frequency $2\sqrt{m}g$, increasing with the rung number m . In the limit of vanishing pumping $W \ll \Gamma_C$, the luminescence spectrum is determined by transitions from the lowest occupied excited levels $|1, \pm\rangle$ to the ground state $|0\rangle$, and therefore contains two peaks at the frequencies $\omega_0 \pm g$ (vacuum Rabi splitting [12]), see Fig. 1*c*. The detailed study of the luminescence spectra at higher pumping intensities can be found in Ref. [34]. The presence of the split level $|1, \pm\rangle$ also results in oscillations of the photon–photon correlator, see Fig. 1*e*. The frequency of the oscillations is $2g$, which allows interpreting them as Rabi oscillations between photon and exciton states.

To illustrate the difference between these emission characteristics and those in the case of resonant pumping, we consider the simplest 3-level scheme, see Fig. 1*b*. Such a scheme may be used for atomic cavity systems [4, 27]. For this, we add a new ground state $|I\rangle$ to the system, while the transition between levels $|X\rangle$ and $|G\rangle$ remains strongly coupled to the cavity mode. The pumping is performed by the coherent external field that resonantly excites the system from the state $|I\rangle$ to the state $|X\rangle$. This can be described by adding the term

$$V = \frac{\Omega}{2} (|X\rangle \langle I| + |I\rangle \langle X|) \quad (11)$$

to Hamiltonian (1), where Ω is the Rabi frequency corresponding to the pumping field. We also introduce the decay rates Γ_{IX} and Γ_{IG} from the respective states $|X\rangle$ and $|G\rangle$ to the state $|I\rangle$. They are taken into account by adding the terms $\Gamma_{IX}L_{|I\rangle\langle X}[\rho]$ and $\Gamma_{IG}L_{|I\rangle\langle G}[\rho]$ to Liouvillian (2). The eigenstates of the total Hamiltonian taking pumping term (11) into account are

$$|0\rangle = |0, G\rangle, \quad |m, C\rangle = \frac{|m-1, I\rangle - \alpha_m |m, G\rangle}{\sqrt{1 + \alpha_m^2}}, \quad (12)$$

$$|m, \pm\rangle = \frac{1}{\sqrt{2}} \left(\frac{|m, G\rangle + \alpha_m |m-1, I\rangle}{\sqrt{1 + \alpha_m^2}} \pm |m-1, X\rangle \right),$$

where $\alpha_m = \Omega/(2\sqrt{m}g)$ describes the pumping-induced state intermixture strength. The energy spectrum forms the Jaynes–Cummings ladder with each rung now consisting of three states,

$$E_0 = 0, \quad E_{m,C} = m\hbar\omega_0, \quad (13)$$

$$E_{m,\pm} = m\hbar\omega_0 \pm \hbar\sqrt{mg^2 + (\Omega/2)^2}.$$

In the case of low pumping $\Omega \ll g$, the state $|1, C\rangle$, which is close to the ground state $|0, I\rangle$, is occupied with a probability close to unity. The luminescence spectrum is determined by transitions from the state $|1, C\rangle$ to $|0\rangle$ (due to an admixture of $|1, G\rangle$ to $|1, C\rangle$), and from $|2, C\rangle$ to $|1, C\rangle$. Contributions from both these transitions are linear in the pumping intensity. Since both transitions occur at the frequency ω_0 , the luminescence spectrum has the only peak at ω_0 , see Fig. 1*d*. The dependence $g^{(2)}(t)$ is plotted in Fig. 1*f*. We can see that the oscillations with the frequency of the vacuum Rabi splitting $2g$ are strongly suppressed in contrast to the case of incoherent pumping considered above.

Thus, we have shown that both the luminescence spectrum and the $g^{(2)}(t)$ dependence are crucially different for the incoherent and coherent pumping regimes. More complex atomic cavity systems with more atomic levels and more complicated resonance pumping schemes have been studied in experimental and theoretical works [4, 21, 22, 27]. To the best of our knowledge, despite the strong-coupling regime, oscillations of the correlator $g^{(2)}(t)$ with the frequency of the vacuum Rabi splitting $2g$ have not been observed in any of these systems.

4. EFFECT OF PUMPING INTENSITY

In this section, we analyze the time dependence $g^{(2)}(t)$ for the incoherently pumped quantum dot strongly coupled to the cavity mode. We first present a general overview of the results and then provide a detailed analytic description in different regimes, determined by the pumping strength.

Our main calculation results are summarized in Fig. 2. Panel *a* shows the dynamics of the correlator $g^{(2)}(t)$, and panels *b* and *c* present the average lifetime of the correlations

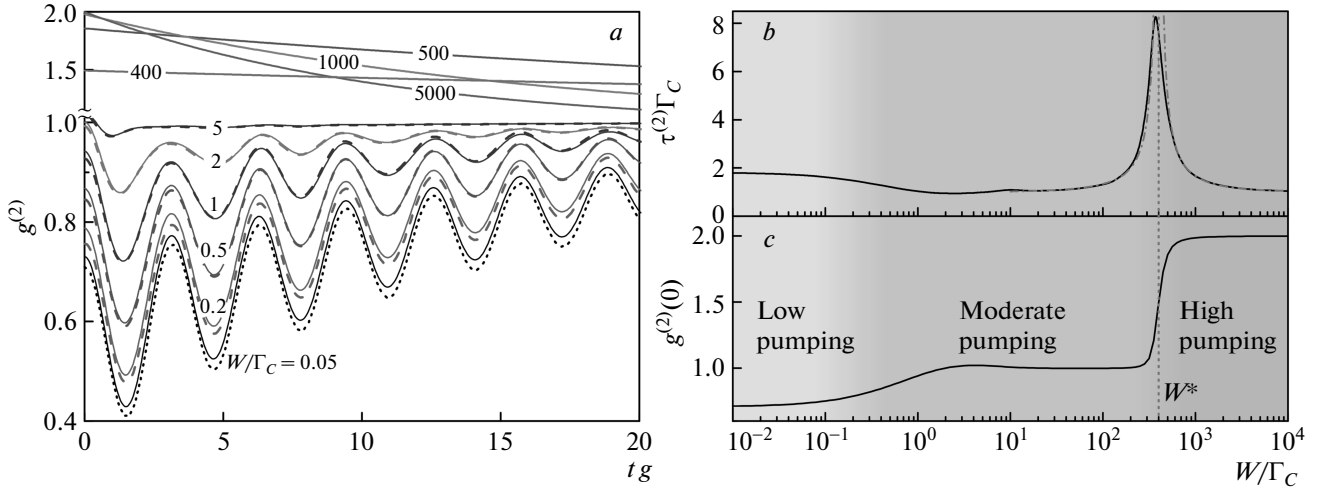


Fig. 2. *a)* Time dependence of the correlation function $g^{(2)}(t)$ in the strong-coupling regime, $g/\Gamma_C = 10$. The curves are plotted for $\Gamma_X = 0.1\Gamma_C$ and various pumping rates W/Γ_C shown in the graph. Solid lines are obtained numerically. The dotted line corresponds to the low pumping regime and is plotted in accordance with Eq. (15). Dashed lines represent analytic results in the case of moderate pumping and are plotted in accordance with Eq. (19). Panels *b* and *c* respectively show the correlation function decay time calculated in accordance with Eq. (14) and the stationary correlator $g^{(2)}(0)$ as functions of the pumping. The titles correspond to the regimes analyzed in Sec. 4. The dotted vertical line indicates the value of the critical pumping $W^* = 4g^2/\Gamma_C = 400 \Gamma_C$, where the sharp peak of the correlation lifetime $\tau^{(2)}$ occurs. The asymptotic behavior of the time $\tau^{(2)}$ near the critical point plotted in accordance with Eq. (22) is shown by the dash-dotted curve

$$\tau^{(2)} = \int_0^\infty dt [g^{(2)}(t) - 1]t / \int_0^\infty dt [g^{(2)}(t) - 1] \quad (14)$$

and the stationary value $g^{(2)}(0)$. Figure 2 demonstrates that the dependence of the time-resolved correlations on pumping is not trivial. In Secs. 4.1–4.3, the following qualitatively different regimes are described:

A. Low pumping, $W \ll \Gamma_C$. In this case, the correlation function $g^{(2)}(t)$ is less than unity at $t = 0$ (anti-bunching) and demonstrates Rabi oscillations with the frequency $2g$. The decay rate of the oscillations is equal to the average of the exciton and photon decay rates.

B. Moderate pumping, $\Gamma_C \lesssim W \ll g^2/\Gamma_C$. Growth of the pumping intensity leads to the decrease in both the period and the lifetime of the oscillations. In a wide range of higher pumping intensities $\Gamma_C \ll W \ll g^2/\Gamma_C$, the emission statistics is Gaussian and the correlation function is close to unity and almost time-independent. This can be understood as a lasing regime for the dot strongly coupled to the cavity mode.

C. High pumping. The pumping value $W^* = 4g^2/\Gamma_C$ corresponds to the transition from the lasing regime to the so-called self-quenching regime [27]. As the pumping rate crosses the critical point W^* , the stationary correlator $g^{(2)}(0)$ exhibits an abrupt growth,

while the correlation lifetime $\tau^{(2)}$ demonstrates non-monotonic behavior with a sharp peak. It increases as $\tau^{(2)} \propto 1/|W - W^*|$ near the critical point $W = W^*$. The peak height is of the order of g/Γ_C^2 , and much larger than the value of the correlation time in all other regimes.

At large pumping $W \gg W^*$, the strong-coupling regime is destroyed: the emission statistics is thermal [$g^{(2)}(0) = 2$] and the decay time of the correlations is equal to the empty-cavity mode lifetime $1/\Gamma_C$.

We now proceed to a more detailed analysis of regimes (A)–(C).

4.1. Low pumping, $W \ll \Gamma_C$

In the limit of vanishing pumping $W \ll \Gamma_C$, it is sufficient to take only the rungs of Jaynes–Cummings ladder (10) with $m \leq 2$ particles into account. This yields the correlation function

$$g^{(2)}(t) = 1 - \frac{3\Gamma_C - \Gamma_X - (\Gamma_C + \Gamma_X) \cos 2gt}{2(3\Gamma_C + \Gamma_X)} \times \exp\left\{-\frac{(\Gamma_C + \Gamma_X)t}{2}\right\}. \quad (15)$$

Equation (15) shows oscillations of the photon–photon correlator. This is a direct manifestation of the strong-coupling regime. Due to the photon–exciton interaction g , the photon is fully converted into the exciton and vice versa every period $\pi/(2g)$ (Rabi oscillations). This results in the contribution to the correlator, oscillating with the Rabi frequency of the first rung $(E_{1,+} - E_{1,-})/\hbar = 2g$. The decay rate of the Rabi oscillations is the mean of the photon and exciton decay rates $(\Gamma_C + \Gamma_X)/2$. This is also a manifestation of strong coupling and shows formation of the exciton polaritons. For realistic cavities, $\Gamma_C \gg \Gamma_X$ [12] which means that $g^{(2)} \approx 2/3 < 1$ (antibunching) [29]. The black-dotted curve in Fig. 2a is plotted in accordance with Eq. (15) and well reproduces the numerical results for a low pumping rate (the black solid curve).

4.2. Moderate pumping, $\Gamma_C \lesssim W \ll g^2/\Gamma_C$

For moderate pumping, in contrast to the low pumping case (Sec. 4.1), it is necessary to take all the rungs into account. First, we must determine the stationary density matrix $\rho^{(0)}$. As shown in Appendix A, this matrix $\rho^{(0)}$ is diagonal in the basis of states (9) and has the elements $\rho_{0;0}^{(0)} = f_0^{(0)}$, $\rho_{m,\pm;m,\pm}^{(0)} = f_m^{(0)}$, where the distribution function $f_m^{(0)}$ is

$$f_m^{(0)} = \frac{\sqrt{\pi}}{2E(w) + 1} \frac{w^m}{\Gamma(m + 1/2)}. \quad (16)$$

Here, $w = W/2\Gamma_C$ is the dimensionless pumping, and $E(w) = e^w \sqrt{\pi w} \operatorname{erf} \sqrt{w}$, $\Gamma(x)$ and $\operatorname{erf}(x)$ are the gamma and error functions. For simplicity in this section, the exciton decay rate Γ_X is neglected, because $\Gamma_X \ll \Gamma_C$ for typical microcavities [12, 36]. Equation (16) generalizes the analytic result for the distribution function obtained in Ref. [34].

Distribution Eq. (16) yields the following expressions for the particle numbers and the stationary correlator $g^{(2)}(0)$:

$$N_X = \frac{E}{2E + 1}, \quad N_C = 2w \frac{E + 1}{2E + 1}, \quad (17)$$

$$g^{(2)}(0) = \frac{(2E + 1)[4w^2(E + 1) + E - 2w]}{8w^2(E + 1)^2}.$$

Solid curves in Figs. 3a,b,c show the dependence of N_X , N_C , and $g^{(2)}(0)$ on the pumping rate. The curves are presented at different values of the exciton–photon coupling strength g . The results in Figs. 3a,b,c agree with those obtained numerically in Ref. [28]. Here, we focus on the strong-coupling regime (black curves); the

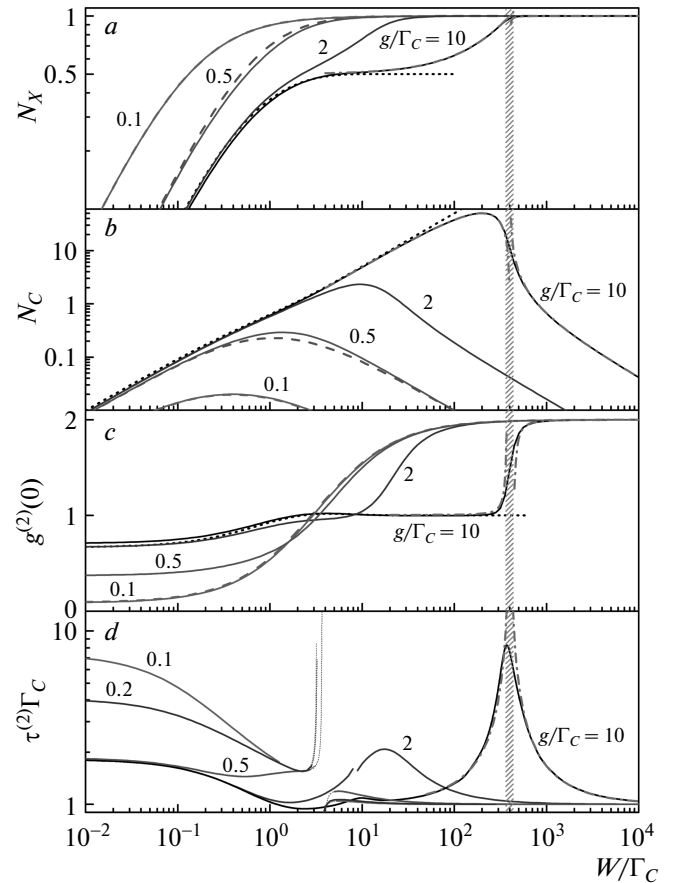


Fig. 3. Dependence on the pumping rate W of (a) the exciton number N_X , (b) the photon number N_C , (c) the correlation function $g^{(2)}(0)$, and (d) the correlation decay time $\tau^{(2)}$, plotted for various coupling strengths g and $\Gamma_X = 0.1\Gamma_C$. Solid lines are obtained from the numerical calculation. Dashed lines in panels a–c represent the weak-coupling regime and are plotted in accordance with Eqs. (23) and (24), while dotted lines correspond to the strong-coupling limit, Eqs. (17). Dash-dotted lines in panels a–d show the analytic results obtained in high pumping regime (20) and (22) and valid outside the patterned region $|W - W^*| \sim 4g = 40\Gamma_C$ for the parameters chosen. Thin dotted lines in panel d correspond to the range of pumping where the function $g^{(2)}(t)$ is close to unity and the definition of $\tau^{(2)}$ according to Eq. (14) fails

weak coupling case is analyzed in Sec. 5. The dot population N_X (see Fig. 3a) monotonically increases at low pumping as $N_X = W/\Gamma_C$ and reaches a plateau $N_X = 1/2$ at $W \sim \Gamma_C$. The plateau $N_X = 1/2$ reflects the half-exciton–half-photon nature of polariton eigenstates Eq. (9) with $m \geq 1$. The photon number N_C (see Fig. 3b) linearly increases for low and moderate

pumping as $N_C = W/\Gamma_C$ and $N_C = W/(2\Gamma_C)$ respectively. The second-order correlator $g^{(2)}(0)$ (see Fig. 3c) increases with the pumping and reaches the plateau $g^{(2)}(0) = 1$ at $W \sim \Gamma_C$ (the lasing regime [27, 34]). In the moderate pumping regime, all the curves N_X , N_C , and $g^{(2)}(0)$ are well described by Eq. (17) (see black dotted curves).

We now proceed to the discussion of the dynamics of $g^{(2)}(t)$. Two independent contributions can be singled out in the time dependence (see Fig. 2a): (i) the oscillatory contribution and (ii) the monotonically decaying contribution. As shown in Appendix A, the oscillatory term demonstrates a superposition of the Rabi beatings between the split states inside different rungs of the Jaynes–Cummings ladder with the frequencies $2\sqrt{m}g$. The weight of the term corresponding to the rung m is determined by the distribution function $f_{m+1}^{(0)}$. The damping of the oscillations is due to the stimulated photon decay and exciton pumping and is equal to $\Gamma_C(m - 1/2) + W/2$. The nonoscillating term decays in time toward unity on the time scale of Γ_C . Calculation shows that this decay can be approximated as an exponential one with the rate

$$\Gamma_1 = \Gamma_C \left[1 - \frac{2w - 1}{4w(E + 1)} - \frac{(2w - 1)^2}{4w(2E + 1)} \right]^{-1}. \quad (18)$$

For small pumping $W \ll \Gamma_C$, Eq. (18) reduces to $\Gamma_1 = \Gamma_C/2$, whereas for moderate pumping $W \gg \Gamma_C$, we obtain $\Gamma_1 = \Gamma_C$. The resulting expression for the correlator $g^{(2)}(t)$ assumes the form

$$g^{(2)}(t) = 1 - \frac{1}{2(E + 1)} e^{-\Gamma_1 t} + \frac{1}{2N_C^2} \sum_{m=1}^{\infty} f_{m+1}^{(0)} \cos(2\sqrt{m}gt) \times \exp \left\{ - \left[\Gamma_C \left(m - \frac{1}{2} \right) + W/2 \right] t \right\}. \quad (19)$$

For low pumping, the sum in Eq. (19) is determined by the first term with $m = 1$ and the result agrees with Eq. (15) assuming that $\Gamma_X = 0$.

Analytic results plotted in accordance with Eq. (19) are shown in Fig. 2a by dashed curves. The difference from the exact calculation at small pumping is due to the neglected exciton decay rate Γ_X . Equation (19) well reproduces the main features of the numerically calculated dependence: for larger pumping, the oscillations amplitude significantly decreases and the oscillations decay faster. This is a characteristic feature of the two-level system, distinct from the boson system where the lifetime of fluctuations increases with pumping [37, 38].

4.3. High pumping, $W \sim 4g^2/\Gamma_C$

When the pumping rate increases to $W \sim g^2/\Gamma_C$, the exciton level broadening caused by pumping becomes comparable to the rung splitting. This results in saturation of the exciton number at unity (see Fig. 3a) and a drastic decrease in the photon number (see Fig. 3b).

A detailed description of the stationary density matrix and correlator dynamic equations is given in Appendix B. It is shown that the emission statistics changes qualitatively when the pumping rate crosses the critical value $W^* = 4g^2/\Gamma_C$. For lower-than-critical pumping, the distribution function is Gaussian, while for larger pumping it becomes thermal. The transition occurs in the vicinity of the critical point $|W - W^*| \lesssim 4g$. Below, we present analytic expressions for emission characteristics valid outside this narrow region.

The static characteristics for $|W - W^*| \gtrsim 4g$ are given by

$$N_X = \begin{cases} \frac{1 + W/W^*}{2}, & W < W^* \\ 1 - \frac{\Gamma_C}{W(W/W^* - 1)}, & W > W^*, \end{cases} \quad (20)$$

$$N_C = \begin{cases} \frac{W}{2\Gamma_C}(1 - W/W^*), & W < W^*, \\ \frac{1}{W/W^* - 1}, & W > W^*, \end{cases}$$

$$g^{(2)}(0) = \begin{cases} 1 + \frac{2\Gamma_C}{W^*(1 - W/W^*)^2}, & W < W^*, \\ 2 - \frac{4\Gamma_C}{W(1 - W^*/W)^2}, & W > W^*. \end{cases}$$

Dash-dotted lines in Figs. 3a,b,c present the dependence of N_X , N_C , and $g^{(2)}(0)$ on the pumping rate near the critical point W^* plotted in accordance with Eq. (20). We can see a perfect agreement of the analytic results with the numerical calculation (the black solid curve) outside the narrow patterned transition region.

The time dependence of the correlator $g^{(2)}(t)$ is mono-exponential,

$$g^{(2)}(t) = 1 + [g^{(2)}(0) - 1] e^{-t/\tau^{(2)}}, \quad (21)$$

where the correlation lifetime is given by

$$\tau^{(2)} = \frac{1}{\Gamma_C} \begin{cases} \frac{1}{1 - W/W^*}, & W < W^*, \\ \frac{1}{1 - W^*/W}, & W > W^*. \end{cases} \quad (22)$$

Equation (22) shows that the correlation lifetime drastically increases near the critical point $W = W^*$. Its maximum value can be estimated from Eq. (22) by substituting $|W - W^*| = 4g$, which gives the value $\tau^{(2),max} = g/\Gamma_C^2$, which is larger than the correlation lifetime in all other regimes by the factor g/Γ_C . The dependence of the lifetime $\tau^{(2)}$ on the pumping rate near the critical point W^* is shown in Fig. 3d by the dash-dotted line.

The origin of the peak in the correlation lifetime at $W = W^*$ can be qualitatively understood as follows. At $W > W^*$, the strong-coupling regime is already destroyed due to the self-quenching. But if $W - W^* \ll \ll W^*$, then the number of photons in the cavity is still large (see Eq. (20)). Hence, this system can be viewed as a conventional weakly coupled laser, where the fluctuation lifetime is increased due to the boson stimulation factor, $\tau^{(2)} = (N_C + 1)/\Gamma_C$ [37, 38]. For a single dot in the cavity, such a decay time enhancement can be realized only at strong coupling, because in the weak coupling case, the number of photons remains small at any pumping (see Fig. 3b and Sec. 5 below).

5. WEAK COUPLING REGIME

In this section, we analyze quantum dot microcavities where the strong-coupling condition $g \gg \Gamma_C$, Γ_X is violated. Figures 3a,b,c,d show the dependence of the particle numbers, the stationary two-photon correlator, and the correlation lifetime on the coupling strength. A decrease in the coupling strength parameter g/Γ_C suppresses the maximal number of photons and the peak value of $\tau^{(2)}$, and also shifts the self-quenching transition to lower values of the pumping (curves ($g/\Gamma_C = 2$) in Fig. 3). As soon as the coupling strength g becomes smaller than Γ_C , the regime of weak coupling between the photon and the exciton is realized. At weak coupling, the number of photons is much less than unity at any pumping, as can be clearly seen from the curve ($g/\Gamma_C = 0.1$) in Fig. 3b.

The smallness of the photon number allows considering only the lowest levels of the system when deriving analytic results. Hence, we take states with no more than one photon into account when calculating photon number and dot occupation, and states with up to two photons for the photon–photon correlator. Analytic expressions for the particle numbers in the weak-coupling regime are [39]

$$N_X = \frac{W[4g^2 + \Gamma_C(W + \Gamma_C + \Gamma_X)]}{(W + \Gamma_C + \Gamma_X)[4g^2 + \Gamma_C(W + \Gamma_X)]}, \quad (23)$$

$$N_C = \frac{4g^2W}{(W + \Gamma_C + \Gamma_X)[4g^2 + \Gamma_C(W + \Gamma_X)]}$$

At low pumping, both N_X and N_C increase linearly with pumping. At large pumping, the dot is completely populated, $N_X = 1$, while the cavity is empty ($N_C \rightarrow 0$) due to the self-quenching effect (see Figs. 3a,b).

An analytic expression for $g^{(2)}(0)$ in the “bad” cavity regime ($g \ll \Gamma_C$) is

$$g^{(2)}(0) = 2 \frac{W + \Gamma_X + 4g^2/\Gamma_C}{W + \Gamma_X + 3\Gamma_C}. \quad (24)$$

In the limit of vanishing pumping and $\Gamma_X \ll \ll \Gamma_C, g^2/\Gamma_C$, the value of $g^{(2)}(0)$ is smaller than the strong-coupling limit $2/3$. With a decrease in the coupling strength g , antibunching becomes stronger due to a smaller admixture of photons to the exciton state.

With an increase in the pumping rate the initial value $g^{(2)}(0)$ increases from zero (antibunching) to 2 (thermal regime) (see Fig. 3c). The lasing regime with a plateau at $g^{(2)}(0) = 1$ is destroyed in the weak-coupling case. Shown in the Figs. 3a,b,c by the dashed lines is the analytic dependence plotted in accordance with Eqs. (23) and (24). We can see a perfect agreement with the numerical calculation shown by the solid lines.

The time dependence $g^{(2)}(t)$ is calculated in accordance with the procedure defined by Eq. (7). For simplicity, we neglect the exciton damping ($\Gamma_X = 0$) and consider only the two limit cases of low and high pumping compared with the spontaneous decay rate of the exciton $4g^2/\Gamma_C$. At the low pumping, we obtain

$$g^{(2)}(t) = 1 - e^{-4g^2t/\Gamma_C}. \quad (25)$$

The system demonstrates antibunching similar to the case of the quantum dot without a cavity. The only effect of the cavity is the enhancement of the exciton decay rate due to the Purcell effect. In the opposite case of high pumping, $W \gg g^2/\Gamma_C$, we obtain

$$g^{(2)}(t) = 1 - \frac{\Gamma_C^2}{(W - \Gamma_C)^2} \times$$

$$\times \left[\frac{2W(W - 5\Gamma_C)}{\Gamma_C(W + 3\Gamma_C)} e^{-(W+\Gamma_C)t/2} + \right.$$

$$\left. + \frac{W(2\Gamma_C^2 + 3W\Gamma_C - W^2)}{\Gamma_C^2(W + 3\Gamma_C)} e^{-\Gamma_C t} + e^{-Wt} \right]. \quad (26)$$

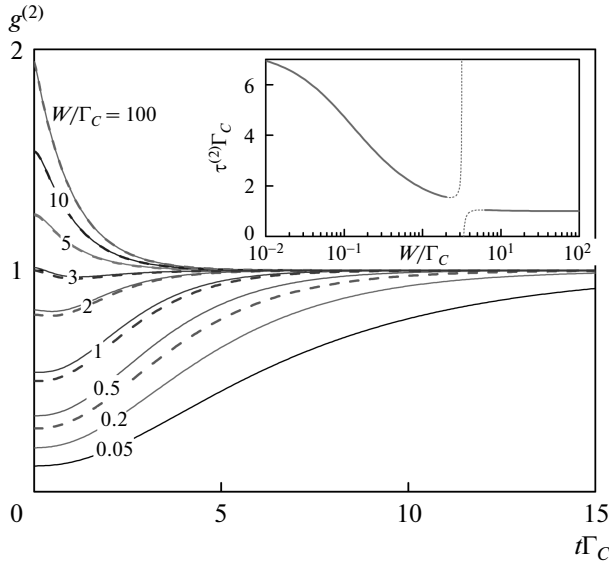


Fig. 4. Time dependence of the correlation function $g^{(2)}(t)$ in the weak-coupling regime, $g/\Gamma_C = 0.1$. Curves are plotted for $\Gamma_X = 0.1\Gamma_C$ and various pumping rates W/Γ_C . Solid lines are obtained from the numerical calculation. Dashed lines represent the moderate pumping case and are plotted in accordance with Eq. (26). The inset shows the pumping dependence of the correlation lifetime $\tau^{(2)}$. The dashed region corresponds to the unphysical divergence in $\tau^{(2)}$ near $W/\Gamma_C = 3$ when $g^{(2)}(t) \approx 1$ and the lifetime in Eq. (14) loses its meaning

We note that Eq. (26) is finite at $W = \Gamma_C$ and reduces to $1 - e^{-\Gamma_C t}(\Gamma_C^2 t^2 + 2\Gamma_C t + 2)/4$ for this particular value of pumping. In Fig. 4, the dependence defined by Eq. (26) is plotted by dashed curves. For the high pumping $W \gg \Gamma_C$, Eq. (26) reduces to $g^{(2)}(t) = 1 + e^{-\Gamma_C t}$. This corresponds to a low number of cavity photons and to thermal statistics. The decay time $\tau^{(2)}$ decreases from $\Gamma_C/(4g^2)$ to $1/\Gamma_C$ as the pumping increases (see Fig. 3d and the inset in Fig. 4). Although the behavior of the decay time at weak coupling is generally monotonic, there is a region of pumping values where $g^{(2)}(t)$ is close to unity (see the wine-colored curve for $W/\Gamma_C = 3$). In this case, the correlation lifetime $\tau^{(2)}$ defined in accordance with Eq. (14) has no sense. Thin dotted lines in Fig. 3d and in the inset of Fig. 4 correspond to this region.

6. SUMMARY

We have developed a theory of time-resolved second-order correlations of photons emitted from an

incoherently stationary pumped microcavity with a single quantum dot strongly coupled to the photon mode. Explicit analytic expressions for the photon number, exciton number, and photon–photon correlator $g^{(2)}(t)$ have been obtained. We have shown that the incoherent pumping scheme, typical for semiconductor systems, leads to qualitatively different correlation dynamics than the resonant pumping scheme. In the case of incoherent pumping, the function $g^{(2)}(t)$ demonstrates oscillations at the frequency of the vacuum Rabi splitting, while such oscillations are strongly suppressed in the case of coherent pumping.

Both the frequency and the decay rate of these oscillations increase as the pumping rate increases. At larger pumping, the dynamics of the correlations is monoexponential. The decay time nonmonotonically depends on the pumping and has a sharp peak at the critical pumping value corresponding to the self-quenching transition between the lasing regime [where $g^{(2)}(0) = 1$] and the thermal regime [$g^{(2)}(0) = 2$]. The peak value strongly exceeds the lifetime of the empty cavity mode. Such a nonmonotonic behavior of the correlation lifetime is a characteristic feature of the cavity with a single dot in the strong-coupling regime.

In the weak-coupling regime, the correlation function almost monotonically changes from the initial value at $t = 0$ to unity at large delays. The value of the zero-delay correlator $g^{(2)}(0)$ in the weak-coupling regime is smaller than unity at low pumping (photon antibunching) and tends to 2 at large pumping (thermal bunching). The increase in pumping shortens the decay time of the photon–photon correlations.

The authors acknowledge numerous fruitful discussions with M. M. Glazov. This work was supported by the RFBR, RF President Grants MD-2062.2012.2 and NSh-5442.2012.2, EU projects SPANGL4Q and POLAPHEN, and the “Dynasty” Foundation.

APPENDIX A

Dynamic equations in the strong-coupling regime

In this Appendix, we present the details of the derivation of analytic answers (16)–(19) for the stationary density matrix and for the time-dependent two-photon correlator. We focus on the strong-coupling regime and the moderate pumping $W \ll 4g^2/\Gamma_C$.

The key simplification in the strong-coupling regime is the smallness of the nondiagonal components of the stationary density matrix. This is so because the en-

ergy width of polariton eigenstates (9) is of the order of $\max(\Gamma_C, W)$ and much less than the splitting $2\sqrt{mg}$ between these states, where m is the relevant rung number of the Jaynes–Cummings ladder. Estimating the typical values of m as W/Γ_C , we obtain the small parameter $\max(\Gamma_C, \sqrt{W\Gamma_C})/g$ for the nondiagonal density matrix elements. We note that for a sufficiently high pumping $W \sim g^2/\Gamma_C$, this parameter is no longer small. The nondiagonal density matrix elements in this case are given by Eq. (B.3) and their effect is discussed in detail in Appendix B.

Thus, in the regime of moderate pumping, we can consider the dynamics of diagonal and nondiagonal density matrix elements separately. The kinetic equation for the diagonal elements $f_m = \rho_{m,+;m,+} = \rho_{m,-;m,-}$, $f_0 = \rho_{0,0}$ is obtained from Liouvillian (2) and is given by

$$\begin{aligned} \frac{df_m}{dt} &= -\frac{W}{2}(f_m - f_{m-1}) - \frac{\Gamma_X}{2}(f_m - f_{m+1}) - \\ &\quad - \Gamma_C[(m-1/2)f_m - (m+1/2)f_{m+1}], \quad (\text{A.1}) \\ \frac{df_0}{dt} &= -Wf_0 + (\Gamma_X + \Gamma_C)f_1. \end{aligned}$$

A stationary solution of this equation can be found using the fact that the probability flow between the two adjacent rungs m and $m+1$ should be zero, i. e.,

$$-\frac{W}{2}f_m^{(0)} + \frac{\Gamma_X}{2}f_{m+1}^{(0)} + \Gamma_C\left(m + \frac{1}{2}\right)f_{m+1}^{(0)} = 0. \quad (\text{A.2})$$

This yields the probability distribution

$$f_m^{(0)} \propto \frac{(W/2\Gamma_C)^m}{\Gamma(m+1/2 + \Gamma_X/2\Gamma_C)}, \quad (\text{A.3})$$

which should be normalized as

$$f_0^{(0)} + 2 \sum_{m=1}^{\infty} f_m^{(0)} = 1. \quad (\text{A.4})$$

Hereinafter, we neglect the exciton damping for simplicity, $\Gamma_X = 0$. In this case, Eqs. (A.3) and (A.4) lead to Eq. (16). The stationary photon (N_C) and exciton (N_X) numbers and the two-photon correlator $g^{(2)}(0)$ are readily found from the distribution $f_m^{(0)}$:

$$N_X = \sum_{m=1}^{\infty} f_m^{(0)}, \quad N_C = \sum_{m=1}^{\infty} f_m^{(0)}(2m-1), \quad (\text{A.5})$$

$$g^{(2)}(0) = \frac{2}{N_C^2} \sum_{m=2}^{\infty} f_m^{(0)}(m-1)^2, \quad (\text{A.6})$$

which yields Eqs. (17).

The time dynamics of $g^{(2)}(t)$ is governed by Eq. (7). We must determine the time dependence of the operator $\chi(t) \equiv e^{\mathcal{L}t}[c\rho_0c^\dagger]$. This operator can be split into

diagonal and nondiagonal parts in the basis of polariton eigenstates: $\chi_{0;0} = \chi_0^{(d)}$, $\chi_{m,\pm;m,\pm} = \chi_m^{(d)}$ (diagonal part), and $\chi_{m,+;m,-} = \chi_{m,-;m,+}^* = \chi_m^{(nd)}$ (nondiagonal part). These two parts evolve independently in the strong coupling and moderate pumping regime. Correlation function (6) can be expressed in terms of the matrix elements as

$$\begin{aligned} g^{(2)}(t) &= \frac{1}{N_C^2} \times \\ &\quad \times \sum_{m=1}^{\infty} \left[(2m-1)\chi_m^{(d)}(t) + \text{Re} \chi_m^{(nd)}(t) \right]. \quad (\text{A.7}) \end{aligned}$$

The initial conditions at $t=0$ is

$$\begin{aligned} \chi_0^{(d)}(0) &= f_1^{(0)}, \quad \chi_m^{(d)}(0) = (m+1/2)f_{m+1}^{(0)}, \\ \chi_m^{(nd)}(0) &= f_{m+1}^{(0)}/2, \quad m \geq 1. \end{aligned} \quad (\text{A.8})$$

Below, we first consider the time dynamics of the diagonal matrix elements, and then analyze the nondiagonal ones.

Diagonal elements satisfy Eqs. (A.1), where f_m should be replaced with $\chi_m^{(d)}$. To determine their time dependence, we analyze the eigenvectors and eigenvalues of this linear system. The largest eigenvalue is zero and corresponds to the stationary distribution function $f_m^{(0)}$. All other eigenvalues are negative and describe solutions decaying with time. Our goal is to provide an estimation for the nonzero eigenvalue with the smallest absolute value Γ_1 . Comparison with the numerical calculation demonstrates that this single eigenvalue satisfactorily describes the dynamics of the diagonal matrix elements $\chi^{(d)}(t)$.

The Lindblad-type matrix corresponding to the right-hand side of Eqs. (A.1) is not Hermitian. The problem can be still reduced to a Hermitian one by the procedure adopted for kinetic and Fokker–Planck equations [40]. In our case, this procedure is formally equivalent to defining the scalar product of two distributions u_m and v_m as

$$(u, v) \equiv \frac{u_0v_0}{f_0^{(0)}} + 2 \sum_{m=1}^{\infty} \frac{u_mv_m}{f_m^{(0)}}. \quad (\text{A.9})$$

In terms of scalar product (A.9), the operator corresponding to the right-hand side of Eqs. (A.1), denoted by a dot in what follows, turns out to be self-adjoint, $(u, \dot{v}) = (\dot{u}, v)$ for any distributions u_m and v_m . This allows analyzing kinetic equations (A.1) by the standard approaches of quantum mechanics. For instance, normalization condition (A.4) takes the compact form $(f^{(0)}, f^{(0)}) = 1$.

From the considered distribution $\chi_m^{(d)}$, it is convenient to single out the stationary contribution $(f^{(0)}, \chi^{(d)}) f_m^{(0)}$ that corresponds to the zero eigenvalue. This yields

$$\chi_m^{(d)}(t) = N_C f_m^{(0)} + \delta\chi_m^{(d)}(t). \quad (\text{A.10})$$

Initial conditions for the new variables $\delta\chi_m^{(d)}(t)$ are given by

$$\delta\chi_0^{(d)}(0) = \frac{2Ewf_0^{(0)}}{2E+1}, \quad \delta\chi_m^{(d)}(0) = -\frac{wf_m^{(0)}}{2E+1}. \quad (\text{A.11})$$

Since the projection of $\delta\chi^{(d)}$ onto the stationary solution $(\delta\chi^{(d)}, f^{(0)})$ is zero, $\delta\chi^{(d)}(t)$ vanishes at large times, which allows verifying that $g^{(2)}(t) \rightarrow 1$ as $t \rightarrow \infty$. Approximating the time decay as $\delta\chi^{(d)}(t) = \delta\chi^{(d)}(0)e^{-\Gamma_1 t}$ and substituting Eqs. (A.10) and (A.11) in Eq. (A.7), we obtain the first two terms in the right-hand side of Eq. (19). Here, Γ_1 is the desired eigenvalue governing the time decay of $\delta\chi^{(d)}$. It can be estimated using the following variational ansatz for the corresponding eigenvector:

$$f_m^{(1)} = f_m^{(0)}(1 + \alpha m), \quad m \geq 0. \quad (\text{A.12})$$

The constant α is found by imposing the orthogonality condition $(f^{(1)}, f^{(0)}) = 0$. Once α is found, the value of Γ_1 is given by

$$\Gamma_1 = \frac{(f^{(1)}, \dot{f}^{(1)})}{(f^{(1)}, f^{(1)})}. \quad (\text{A.13})$$

The result of calculations reduces to Eq. (18).

We now turn to the evolution of the nondiagonal matrix elements $\chi_m^{(nd)}$. In the strong-coupling regime, this procedure is quite simple. We can assume that each matrix element $\chi_m^{(nd)}(t)$ oscillates in time with its own frequency $(E_{m,+} - E_{m,-})/\hbar = 2\sqrt{m}g$ and decays exponentially. The intermixing of different rungs can be neglected if the frequency difference between the adjacent rungs $E_{m+1,+} - E_{m,+} \sim g(\sqrt{m+1} - \sqrt{m})$ is smaller than the coupling term, which is of the order of the pumping strength W . This is realized for $W \ll g^{2/3}\Gamma_C^{1/3}$, i. e., below the transition to the lasing regime [34]. We note that in the polariton lasing regime, $g^{(2)}(0) = 1$ (see Eq. (17)) and the photon correlator dynamics is trivial, $g^{(2)}(t) \equiv 1$. Therefore, this case does not need any special consideration. Hence, the desired time dependence of $\chi_m^{(nd)}$ is described as

$$\chi_m^{(nd)}(t) = \chi_m^{(nd)}(0) e^{-2i\sqrt{m}gt} \times \exp\left\{-\left[\Gamma_C\left(m - \frac{1}{2}\right) + W/2\right]t\right\}. \quad (\text{A.14})$$

Substituting the nondiagonal component dynamics defined by Eq. (A.14) in Eq. (A.7), we recover the last term in Eq. (19).

APPENDIX B

Dynamic equations in the self-quenching regime

Here, we present the details of the $g^{(2)}(t)$ correlator dynamics for the system in the strong-coupling regime and under high pumping. We focus on the transition from lasing to the self-quenching regime ($W \sim 4g^2/\Gamma_C$) when the correlation lifetime turns out to be extremely long.

Despite the strong coupling, sufficiently high pumping leads to the intermixing of eigenstates of Hamiltonian (1). Therefore, the density matrix is no longer diagonal in the polariton basis. Inside the m th rung of the Jaynes–Cummings ladder, it can be written as

$$\rho_m = \begin{pmatrix} f_m & x_m \\ x_m^* & f_m \end{pmatrix} \quad (\text{B.1})$$

in the basis of eigenstates in Eq. (9). Liouvillian (2) does not mix the intra-rung and inter-rung density matrix components. Hence, the stationary density matrix, as well as the operator $\chi(t)$ that describes the $g^{(2)}(t)$ dynamics, do not contain inter-rung components.

In the considered regime of high pumping, the density matrix equations for the rung m are given by

$$\begin{aligned} \frac{df_m}{dt} &= \frac{W}{2}[f_{m-1} - f_m + \text{Re}(x_{m-1} - x_m)] + \\ &+ \Gamma_C \left[\left(m + \frac{1}{2}\right) f_{m+1} - \left(m - \frac{1}{2}\right) f_m \right], \quad (\text{B.2}) \\ \frac{dx_m}{dt} &= -2i\sqrt{m}gx_m - W \left(f_m + \frac{3x_m}{4} + \frac{x_m^*}{4} \right). \end{aligned}$$

The diagonal components f_m change with the rate of the order of Γ_C , as is proved later. The nondiagonal component x_m relaxes to its quasistationary value with a much larger rate, of the order of W . Hence, we assume that x_m adiabatically follows the diagonal components f_m , i. e.,

$$x_m = \frac{2i\sqrt{m}gW - W^2/2}{4mg^2 + W^2/2} f_m. \quad (\text{B.3})$$

After substituting expression (B.3) for the nondiagonal components in Eq. (B.2), we obtain

$$\begin{aligned} \frac{df_m}{dt} &= \frac{W}{2}(\xi_{m-1}f_{m-1} - \xi_m f_m) + \\ &+ \Gamma_C \left[\left(m + \frac{1}{2}\right) f_{m+1} - \left(m - \frac{1}{2}\right) f_m \right], \quad (\text{B.4}) \end{aligned}$$

where $\xi_m = m/(m+q)$ and $q = W^2/(8g^2)$. In the moderate pumping case, ξ_m is close to unity and Eq. (B.4) reduces to Eq. (A.1).

Since we consider high rungs, we can replace the discrete rung number m with a continuous variable, which yields

$$\frac{\partial f(m,t)}{\partial t} + \frac{\partial j(m,t)}{\partial m} = 0, \quad (B.5)$$

$$j(m,t) = \Gamma_C m \left[\frac{w-q-m}{m+q} f(m,t) - \frac{\partial f(m,t)}{\partial m} \right],$$

where $j(m,t)$ is the probability current. The stationary solution found from the condition $j(m) = 0$ is

$$f^{(0)}(m) \propto (m+q)^w e^{-m}. \quad (B.6)$$

As the pumping increases, the maximum of stationary distribution function (B.6) behaves as $w - q$. It increases linearly at low pumping, reaches a maximum at $W = 2g^2/\Gamma_C$, then decreases, reaches zero at the critical pumping value $W^* = 4g^2/\Gamma_C$ when $w = q = 2g^2/\Gamma_C^2$, and remains zero for higher pumping.

We first consider the subcritical pumping, $W < W^*$. Stationary distribution function (B.6) can then be approximated as a Gaussian,

$$f^{(0)}(m) = \frac{1}{\sqrt{8\pi w}} \exp \left[-\frac{(m-w+q)^2}{2w} \right]. \quad (B.7)$$

We use distribution function (B.7) for $w - q \gg \sqrt{2w}$ to calculate N_X , N_C , and $g^{(2)}(0)$ according to Eqs. (3) and (8) and taking both diagonal and nondiagonal components of stationary density matrix (B.1) into account. This yields the results presented in the upper parts of Eqs. (20). Time-dependent equation (B.5) reduces to

$$\frac{\partial f(m,t)}{\partial t} = \Gamma_C \bar{m} \frac{\partial}{\partial m} \left[\frac{m-\bar{m}}{w} f(m,t) + \frac{\partial f(m,t)}{\partial m} \right], \quad (B.8)$$

where $\bar{m} = w - q$ is the mean rung number. The dynamics of the correlator $g^{(2)}(t)$ according to Eq. (7) is given by

$$g^{(2)}(t) = \frac{2}{N_C^2} \int_0^\infty m \chi(m,t) dm, \quad (B.9)$$

where $\chi(m,t)$ satisfies dynamic equation (B.8) with the initial condition $\chi(m,0) = m f_0(m)$. This initial condition can be represented as a sum of two contributions: $\bar{m} f^{(0)}(m)$ and $(m - \bar{m}) f^{(0)}(m)$. The first does

not evolve with time and provides the correct limit $g^{(2)}(t) \rightarrow 1$ as $t \rightarrow \infty$, while the second turns out to be the eigenfunction of the right-hand side of Eq. (B.8) with the eigenvalue $-\Gamma_C \bar{m}/w$. Hence, this eigenvalue describes the decay of the correlator $g^{(2)}(t)$ to unity, given in Eq. (21) and the upper part of Eq. (22).

In the opposite case of the pumping rate larger than the critical, $w - q \gg \sqrt{2w}$ ($W > W^*$), stationary distribution function (B.6) reduces to a thermal one,

$$f^{(0)}(m) = \frac{1}{2\bar{m}} e^{-m/\bar{m}}, \quad (B.10)$$

where the mean rung number is now given by $\bar{m} = q/(q-w)$. Using distribution function (B.10), we calculate the analytic expressions for N_X and N_C presented in the lower parts of Eqs. (20). However, in order to obtain a correction to $g^{(2)}(0) = 2$, it is indispensable to take a deviation of the static distribution from thermal into account. This can be done by introducing the factor $1 + (\bar{m}^2 - m^2/2)w/q^2$ into Eq. (B.10). The dynamic equation for the pumping higher than critical then reduces to

$$\frac{\partial f(m,t)}{\partial t} = \frac{\partial}{\partial m} \left[\Gamma_C m \left(\frac{f(m,t)}{\bar{m}} + \frac{\partial f(m,t)}{\partial m} \right) \right]. \quad (B.11)$$

It can be easily verified that $(m - \bar{m}) f^{(0)}(m)$ is again an eigenfunction of the right-hand side of Eq. (B.11). Thus, the decay of the correlator $g^{(2)}(t)$ is governed by the corresponding rate Γ_C/\bar{m} , which leads to Eq. (21) and the lower part of Eq. (22).

REFERENCES

1. A. Kavokin, J. Baumberg, G. Malpuech, and F. Laussy, *Microcavities*, Clarendon Press, Oxford (2006).
2. A. Muller, W. Fang, J. Lawall, and G. S. Solomon, *Phys. Rev. Lett.* **103**, 217402 (2009).
3. A. Dousse, J. Suffczynski, A. Beveratos, O. Krebs, A. Lemaitre, I. Sagnes, J. Bloch, P. Voisin, and P. Senellart, *Nature* **466**, 217 (2010).
4. A. Kuhn and D. Ljunggren, *Contemp. Phys.* **51**, 289 (2010).
5. H. Carmichael, *An Open Systems Approach to Quantum Optics*, Springer, New York (1993).
6. E. del Valle, A. Gonzalez-Tudela, F. P. Laussy, C. Tejedor, and M. J. Hartmann, *Phys. Rev. Lett.* **109**, 183601 (2012).

7. P. Michler, A. Imamoglu, M. D. Mason, P. J. Carson, G. F. Strouse, and S. K. Buratto, *Nature* **406**, 968 (2000).
8. Z. Yuan, B. E. Kardynal, R. M. Stevenson, A. J. Shields, C. J. Lobo, K. Cooper, N. S. Beattie, D. A. Ritchie, and M. Pepper, *Science* **295**, 102 (2002).
9. M. Calic, P. Gallo, M. Felici, K. A. Atlasov, B. Dwir, A. Rudra, G. Biasiol, L. Sorba, G. Tarel, V. Savona et al., *Phys. Rev. Lett.* **106**, 227402 (2011).
10. C. A. Kessler, M. Reischle, F. Hargart, W.-M. Schulz, M. Eichfelder, R. Roßbach, M. Jetter, P. Michler, P. Gartner, M. Florian et al., *Phys. Rev. B* **86**, 115326 (2012).
11. M. Abbarchi, T. Kuroda, T. Mano, M. Gurioli, and K. Sakoda, *Phys. Rev. B* **86**, 115330 (2012).
12. G. Khitrova, H. M. Gibbs, M. Kira, S. W. Koch, and A. Scherer, *Nature Phys.* **2**, 81 (2006).
13. S. Reitzenstein and A. Forchel, *J. Phys. D* **43**, 033001 (2010).
14. M. Nomura, N. Kumagai, S. Iwamoto, Y. Ota, and Y. Arakawa, *Nature Phys.* **6**, 279 (2010).
15. A. Tandraechanurat, S. Ishida, D. Guimard, M. Nomura, S. Iwamoto, and Y. Arakawa, *Nature Photon.* **5**, 91 (2011).
16. C. Schneider, T. Heindel, A. Huggenberger, T. A. Niederstrasser, S. Reitzenstein, A. Forchel, S. Hofling, and M. Kamp, *Appl. Phys. Lett.* **100**, 091108 (pages 4) (2012).
17. H. J. Kimble, *Phys. Scripta* **1998**, 127 (1998).
18. T. Yoshie, A. Scherer, J. Hendrickson, G. Khitrova, H. M. Gibbs, G. Rupper, C. Ell, O. B. Shchekin, and D. G. Deppe, *Nature* **432**, 200 (2004).
19. J. P. Reithmaier, G. Sek, A. Löffler, C. Hofmann, S. Kuhn, S. Reitzenstein, L. V. Keldysh, V. D. Kulakovskii, T. L. Reinecke, and A. Forchel, *Nature* **432**, 197 (2004).
20. M. O. Scully and M. S. Zubairy, *Quantum Optics*, Cambridge University Press, Cambridge, UK (1997).
21. J. McKeever, A. Boca, A. D. Boozer, J. R. Buck, and H. J. Kimble, *Nature* **425**, 268 (2003).
22. A. D. Boozer, A. Boca, J. R. Buck, J. McKeever, and H. J. Kimble, *Phys. Rev. A* **70**, 023814 (2004).
23. H. J. Kimble, M. Dagenais, and L. Mandel, *Phys. Rev. Lett.* **39**, 691 (1977).
24. D. Walls, *Nature* **280**, 451 (1979).
25. M. Hennrich, A. Kuhn, and G. Rempe, *Phys. Rev. Lett.* **94**, 053604 (2005).
26. H. Jabri and H. Eleuch, *Commun. in Theor. Phys.* **56**, 134 (2011).
27. Y. Mu and C. M. Savage, *Phys. Rev. A* **46**, 5944 (1992).
28. E. del Valle, F. P. Laussy, and C. Tejedor, *Phys. Rev. B* **79**, 235326 (2009).
29. E. del Valle and F. P. Laussy, *Phys. Rev. A* **84**, 043816 (2011).
30. D. Press, S. Götzinger, S. Reitzenstein, C. Hofmann, A. Löffler, M. Kamp, A. Forchel, and Y. Yamamoto, *Phys. Rev. Lett.* **98**, 117402 (2007).
31. E. Illes and S. Hughes, *Phys. Rev. B* **81**, 121310 (2010).
32. N. S. Averkiev, M. M. Glazov, and A. N. Poddubnyi, *JETP* **108**, 836 (2009).
33. A. N. Poddubny, M. M. Glazov, and N. S. Averkiev, *New J. Phys.* **15**, 025016 (2013).
34. A. N. Poddubny, M. M. Glazov, and N. S. Averkiev, *Phys. Rev. B* **82**, 205330 (2010).
35. E. T. Jaynes and F. W. Cummings, *Proc. IEEE* **51**, 89 (1963).
36. S. Reitzenstein and A. Forchel, *J. Phys. D: Appl. Phys.* **43**, 033001 (2010).
37. H. Haken, *Z. Physik* **181**, 96 (1964).
38. M. M. Glazov, M. A. Semina, E. Y. Sherman, and A. V. Kavokin, *Phys. Rev. B* **88**, 041309(R) (2013).
39. F. P. Laussy, E. del Valle, and C. Tejedor, *Phys. Rev. B* **79**, 235325 (2009).
40. H. Risken, *The Fokker-Planck Equation. Methods of Solution and Applications*, Springer, Berlin (1989).